Unsymmetrical dizinc complexes as models for the active sites of phosphohydrolases†

Martin Jarenmark,[a] Edit Csapó,[b] Jyoti Singh,[a] Simone Wöckel,[c] Etelka Farkas,[b] Franc Meyer,[c] Matti Haukka[d] and Ebbe Nordlander*[a]

Received 4th December 2009, Accepted 11th May 2010
First published as an Advance Article on the web 4th August 2010
DOI: 10.1039/b925563j

The unsymmetrical dinucleating ligand 2-(*N*-isopropyl-*N*-((2-pyridyl)methyl)aminomethyl)-6-(*N*-(carboxylmethyl)-*N*-((2-pyridyl)methyl)aminomethyl)-4-methylphenol (IPCPMP or L) has been synthesized to model the active site environment of dinuclear metallohydrolases. It has been isolated as the hexafluorophosphate salt H_4IPCPMP$(PF_6)_2 \cdot 2H_2O$ (H_4L), which has been structurally characterized, and has been used to form two different Zn(II) complexes, $[\{Zn_2(IPCPMP)(OAc)\}_2][PF_6]_2$ (**2**) and $[\{Zn_2(IPCPMP)(Piv)\}_2][PF_6]_2$ (**3**) (OAc = acetate; Piv = pivalate). The crystal structures of **2** and **3** show that they consist of tetranuclear complexes with very similar structures. Infrared spectroscopy and mass spectrometry indicate that the tetranuclear complexes dissociate into dinuclear complexes in solution. Potentiometric studies of the Zn(II) : IPCPMP system in aqueous solution reveal that a mononuclear complex is surprisingly stable at low pH, even at a 2 : 1 Zn(II) : L ratio, but a dinuclear complex dominates at high pH and transforms into a dihydroxido complex by a cooperative deprotonation of two, probably terminally coordinated, water molecules. A kinetic investigation indicates that one of these hydroxides is the active nucleophile in the hydrolysis of bis(2,4-dinitrophenyl)phosphate (BDNPP) enhanced by complex **2**, and mechanistic proposals are presented for this reaction as well as the previously reported transesterification of 2-hydroxypropyl *p*-nitrophenyl phosphate (HPNP) promoted by Zn(II) complexes of IPCPMP.

Introduction

The storage and processing of genetic information is of utmost importance for all living organisms. Nature has chosen phosphodiesters for this task due to their resistance to hydrolytic cleavage, with estimated half lives of tens to hundred of thousand to hundred of billions of years for DNA and about 110 years for RNA.[1] To regulate and express this genetic information, organisms need efficient enzymes for cleavage and formation of phosphodiester bonds. In such enzymes, metals are frequently necessary as cofactors.[2–4] Several enzymes have evolved to make use of two and even three metal ions in a cooperative manner to maximize efficiency.[4–6] Among the "biological" metals,[7] zinc stands out as one of the most commonly used to catalyse hydrolysis reactions in nature due to its high Lewis acidity, flexible coordination sphere and lack of associated redox chemistry.[6,8] Examples of multinuclear zinc enzymes that catalyse phosphoester cleavage are phosphotriesterase,[9] alkaline phosphatase,[10] nuclease P1[11] and phospholipase C.[12] A schematic drawing of the structures of the active sites of the two latter enzymes is shown in Fig. 1. To help in the elucidation of the mechanisms involved in phosphoester cleavage, small synthetic coordination complexes have been used as structural and functional models for the active sites of zinc-dependent enzymes.[1,13–18] In addition to revealing details of the function of dinuclear sites, these model complexes may also be

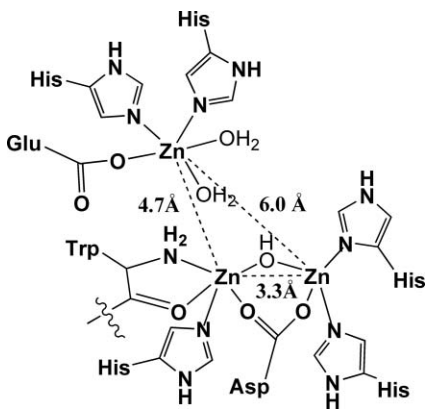

Fig. 1 Schematic drawing of the active site structures of phospholipase C and nuclease P1. The only difference in donors between the two active sites is the substitution of the glutamate for an aspartate in nuclease P1. The metal–metal distances are given for the phospholipase C active site.

[a]*Inorganic Chemistry Research Group, Chemical Physics, Center for Chemistry and Chemical Engineering, Lund University, Box 124, SE-221 00, Lund, Sweden. E-mail: Ebbe.Nordlander@chemphys.lu.se*
[b]*Department of Inorganic and Analytical Chemistry, University of Debrecen, P.O.B. 21, H-4010, Debrecen, Hungary*
[c]*Institute for Inorganic Chemistry, Georg-August-Universität Göttingen, Tammannstrasse 4, D-37077, Göttingen, Germany*
[d]*Department of Chemistry, University of Joensuu, Box 111, FI-80101, Joensuu, Finland*

† Electronic supplementary information (ESI) available: An overlay plot of the molecular structures of complexes **2** and **3** (Fig. S1). Titration curves including fitted curves for the titration of H_4IPCPMP$(PF_6)_2$ (**H_4L**) and mixture of $ZnCl_2$ and L to ratios of 1.5 : 1 and 2 : 1 (Fig. S2). Spectra from ESI-MS+ of mixtures of $ZnCl_2$ and L (2 : 1) with calculated isotope patterns for the species ZnL, Zn_2L, and Zn_2L(OH), and an ESI-MS spectrum of complex **2** (Fig. S3 and S4). Kinetic traces for the HPNP transesterification and BDNPP hydrolysis at various pH. Table of hydrogen bonds in the crystal structure of H_4IPCPMP (Table S1). CCDC reference numbers 659751, 667079 and 755949. For ESI and crystallographic data in CIF or other electronic format see DOI: 10.1039/b925563j

designed to act as artificial restriction enzymes capable of selective cleavage of phosphodiester bonds in DNA or RNA for use in molecular biology.[14,15] Further potential uses include their use as pharmaceuticals directed towards genetic and viral diseases[14] and for detoxification of phosphotriesters and derivatives of these found in some pesticides and chemical warfare reagents.[15]

Despite great efforts, consensus on the exact mechanisms for the various polynuclear metallohydrolases and their models has not yet been reached. The exact roles of the metal ions regarding binding of the substrate, stabilisation of the transition state, and identity of the nucleophile are not perfectly understood although much progress has been made.[6,19,20] The three main proposals for the nucleophilic attack on the phosphorus centre by dinuclear Zn(II) enzymes and biomimetic complexes are shown in Fig. 2, along with the two most commonly discussed suggestions for the binding of the substrate.

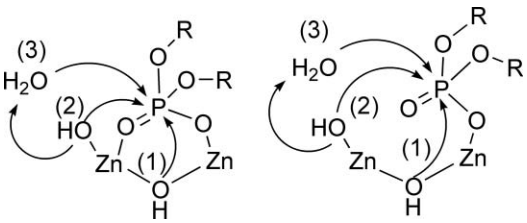

Fig. 2 Mechanistic proposals for the nucleophilic attack on the phosphorus centre in phosphodiester cleavage by dinuclear metalloenzymes and model compounds (active nucleophiles identified by numerals 1–3).[19] All interactions with protein residues have been omitted.

We have developed a number of symmetric and unsymmetric dinucleating ligands (Fig. 3) that include carboxylate groups, a type of donor moiety that is frequently found in the active sites of metallohydrolases. The unsymmetric ligands incorporate a non-coordinating group on one side that (potentially) leaves a vacant coordination site on one of the metals. In enzyme active sites, vacant or solvent-coordinated sites are necessary for facile coordination of the substrate and for activation of solvent-derived nucleophiles.[21] Reaction of $Zn(X)_2{\cdot}2H_2O$ (X = acetate or pivalate) with the dinucleating ligands BCPMP and IPCPMP (*cf*. Fig. 3 for structures of the ligands) leads to the formation of $Na_3[Zn_2(BCPMP)(OAc)_2]_2PF_6 \cdot 6H_2O$ (**1**), $[\{Zn_2(IPCPMP)(OAc)\}_2][PF_6]_2$ (**2**) and $[\{Zn_2(IPCPMP)(O_2CCMe_3)\}_2][PF_6]_2$ (**3**).[22] The solid state structures of **2** and **3** contain tetranuclear "dimer of dimer" complexes, as has been observed for analogous complexes of the ICIMP‡ ligand.[23–25] *In situ* synthesized zinc complexes of IPCPMP also showed higher activity towards transesterification of 2-hydroxypropyl *p*-nitrophenyl phosphate (HPNP, Scheme 1) than **1** did.[22] Here we present the complete procedures for the syntheses of the ligand IPCPMP and complexes **1–3**, an investigation of the solution speciation of complex **2**, and a detailed kinetic investigation of the transesterification of HPNP and the hydrolysis of the organophosphoester 2,4-bis-dinitrophenol-phosphate (BDNPP, Scheme 1) by complex **2**. Parts of these results have been published in an earlier communication.[22]

‡ Ligand abbreviations used in this paper: BCPMP = 2,6-bis[*N*-{*N*-(carboxymethyl)-*N*-(2-pyridylmethyl)amine}methyl]-4-methylphenol, IPCPMP = 2-[*N*-isopropyl-*N*-{(2-pyridyl)methyl}aminomethyl]-6-[*N*-(carboxylmethyl)-*N*-{(2-pyridyl)methyl}aminomethyl]-4-methylphenol (also denoted **L**), BCIMP = 2,6-bis[*N*-{*N*-(carboxymethyl)-*N*-(1-methylimidazolyl)amine}methyl]-4-methylphenol, ICIMP = 2-[*N*-isopropyl-*N*-{(1-methylimidazolyl-pyridyl)methyl}aminomethyl]-6 - [*N*-(carboxylmethyl) - *N* - {(1 - methylimidazolyl)methyl}aminomethyl] - 4-methylphenol

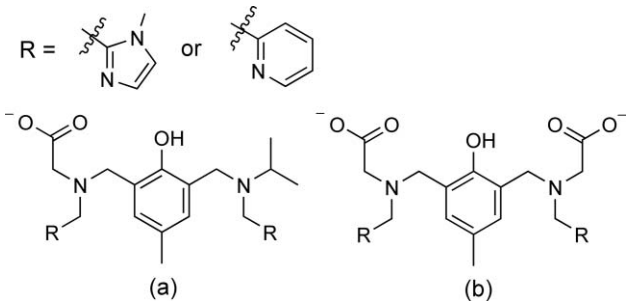

Fig. 3 The four related dinucleating ligands of concern in our studies. R = 2-pyridyl for IPCPMP (a) and BCPMP (b). R = 1-methylimidazolyl for ICIMP (a) and BCIMP (b).

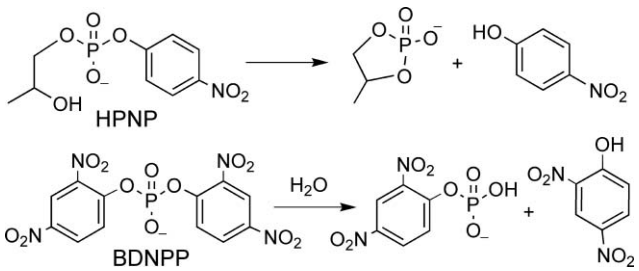

Scheme 1 Transesterification of HPNP (top) and hydrolysis of BDNPP (bottom)

Results and discussion

Synthesis and structure

The ligand IPCPMP (**L**) was assembled *via* modifications of a convergent synthetic protocol (Scheme 2).[22,25,26] The asymmetry of **L** is introduced by the selective oxidation of one of the benzyl

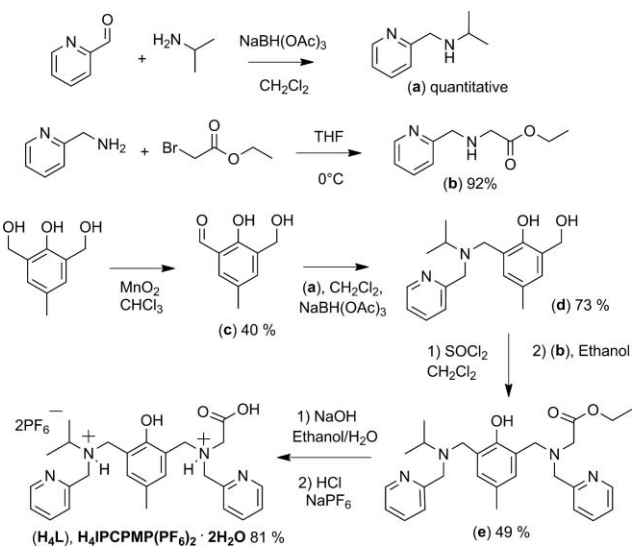

Scheme 2 Synthetic pathway for the ligand IPCPMP

Table 1 Crystallographic data for $H_4IPCPMP(PF_6)_2 \cdot 1.25H_2O$ (**H_4L**) and $[\{Zn_2IPCPMP(OAc)\}_2][PF_6]_2$ (**2**)

	H_4L	**2**
Empirical formula	$C_{104}H_{146}F_{48}N_{16}O_{17}P_8$	$C_{56}H_{66}F_{12}N_8O_{10}P_2Zn_4$
Fw	3052.13	1562.59
T/K	120(2)	120(2)
λ/Å	0.71073	0.71073
Crystal system	Triclinic	Monoclinic
Space group	$P\bar{1}$	$P2_1/c$
a/Å	14.2670(9)	12.5983(2)
b/Å	14.3112(10)	19.4790(3)
c/Å	18.2423(12)	12.5532(4)
α/°	67.849(4)	90
β/°	87.856(3)	97.187(2)
γ/°	69.826(3)	90
V/Å^3	3219.7(4)	3056.38(12)
Z	1	2
ρ_c/Mg m^{-3}	1.574	1.698
μ(Mo-Kα)/mm^{-1}	0.246	1.704
No. reflns.	48041	53314
Unique reflns.	11283	6951
GOOF (F^2)	1.028	1.056
R_{int}	0.1336	0.0375
R_1[a] ($I \geq 2\sigma$)	0.0863	0.0349
wR_2[b] ($I \geq 2\sigma$)	0.1691	0.0897

[a] $R_1 = \sum\|F_o\| - |F_c\|/\sum|F_o|$. [b] $wR_2 = [\sum[w(F_o^2 - F_c^2)^2]/\sum[w(F_o^2)^2]]^{1/2}$.

alcohol moieties using MnO_2. In previous syntheses,[25,26] the side arms were attached sequentially by chlorination of the alcohol group and nucleophilic substitution, followed by reduction of the aldehyde and a second chlorination and substitution to afford the unsymmetric ligand. We have modified this procedure by introducing the first side arm by reductive amination of the aldehyde group using sodium tris(acetoxy)borohydride.[27] This saves two steps although the overall yield is not improved significantly. The yields for the attachment of the ester-containing sidearm are reduced due to the difficulty of separating the product from starting materials. In the final step, the ester group is hydrolysed in aqueous alkali solution. The unsymmetric ligand was isolated by acidification and precipitation as $H_4IPCPMP(PF_6)_2 \cdot H_2O$ (**H_4L**). X-Ray quality crystals were grown from a mixture of methanol and water. Crystallographic data are shown in Table 1 and selected distances for the ligand framework are shown in Table 2 (*cf.* Table S1 in the ESI for hydrogen bonding distances†). The structure of **H_4L** is displayed in Fig. 4, showing the hydrogen-bonding network where two water molecules form bridges between two ligands related by inversion symmetry.

As already mentioned, dinuclear zinc complexes can be formed with IPCPMP in methanol solution if the ligand is deprotonated first. Two complexes were prepared, one containing acetate ($[\{Zn_2(IPCPMP)(OAc)\}_2][PF_6]_2$, **2**) and the other pivalate (trimethylacetate) bridges ($[\{Zn_2(IPCPMP)(O_2CCMe_3)\}_2][PF_6]_2$, **3**). Crystals of X-ray quality could be grown for both complexes. The structure of **3** was briefly presented in a previous report[22] while crystallographic data for **2** can be found in Table 1 and relevant bond distances for both **2** and **3** are shown in Tables 2 and 3. As seen in Fig. 5(a), complex **2** consists of two phenolate-bridged dinuclear entities related by inversion symmetry and bound together by the endogenous (IPCPMP-derived) carboxylates of the ligand. The Zn ions are coordinated in a distorted trigonal bipyramidal geometry (For **2** τ: Zn1 0.77, Zn2 0.52 and for **3** τ: Zn1 0.78, Zn2 0.63, *cf.* ref. 26 for a definition of the τ index).[22,28,29] The carboxylates that bridge the two dinuclear entities bind in a *syn*,*anti*-μ-1,3 manner with the more basic *syn* position[30] coordinated to the other dinuclear part. The structure of **2** is closely related to that of **3** (a structure overlay is shown in Fig. S1 of the ESI†), and similar complexes have previously been structurally characterized for the ligand ICIMP (Fig. 3).[23–25] Overall, the two complexes have quite similar bond lengths, but there is an interesting difference in the bond length for Zn(2)–O(5), which is the bond holding the two dinuclear units together. This bond is much longer in **2** (2.0545(17) Å) than in **3** (1.990 Å), contrary to what may be expected on steric grounds since the less bulky acetates should permit closer approach of the two dinuclear entities. As the difference in bond distances is related to the strength of interaction, this suggests that **2** might be more

Table 2 Bond distances (Å) of the ligand framework in $H_4IPCPMP(PF_6)_2$, $[\{Zn_2(IPCPMP)(OAc)\}_2](PF_6)_2$ (**2**) and $[\{Zn_2(IPCPMP)(Piv)\}_2](PF_6)_2$ (**3**)

	H_4L	**2**	**3**
O1–C8	1.232(7)	1.262(3)	1.265(5)
O2–C8	1.310(7)	1.250(3)	1.247(5)
O3–C16	1.373(7)	1.359(3)	1.355(5)
O4–C27	—	1.259(3)	1.250(5)
O5–C27	—	1.259(3)	1.265(5)
N1–C1	1.335(8)	1.350(3)	1.336(6)
N1–C5	1.359(8)	1.343(3)	1.349(5)
N2–C6	1.474(8)	1.471(3)	1.471(5)
N2–C7	1.451(7)	1.476(3)	1.468(5)
N2–C9	1.468(8)	1.486(3)	1.489(5)
N3–C17	1.518(7)	1.503(3)	1.504(5)
N3–C18	1.553(7)	1.518(3)	1.508(5)
N3–C21	1.478(8)	1.484(3)	1.486(5)
N4–C22	1.327(7)	1.336(3)	1.342(5)
N4–C26	1.334(8)	1.350(3)	1.346(5)
C1–C2	1.352(10)	1.383(4)	1.383(6)
C2–C3	1.382(10)	1.382(4)	1.387(7)
C3–C4	1.368(9)	1.382(4)	1.378(8)
C4–C5	1.362(8)	1.392(3)	1.386(6)
C5–C6	1.479(8)	1.510(3)	1.499(7)
C7–C8	1.477(8)	1.520(3)	1.521(5)
C9–C10	1.489(8)	1.502(3)	1.503(5)
C10–C11	1.385(8)	1.398(3)	1.390(6)
C10–C16	1.405(8)	1.410(3)	1.398(5)
C11–C12	1.381(8)	1.392(3)	1.397(6)
C12–C13	1.502(8)	1.509(3)	1.521(6)
C12–C14	1.394(8)	1.388(4)	1.386(6)
C14–C15	1.380(8)	1.400(3)	1.391(6)
C15–C16	1.386(8)	1.403(3)	1.402(5)
C15–C17	1.509(8)	1.509(3)	1.503(5)
C18–C19	1.512(9)	1.520(4)	1.525(5)
C18–C20	1.497(9)	1.515(4)	1.529(5)
C21–C22	1.510(8)	1.504(4)	1.508(5)
C22–C23	1.381(9)	1.395(4)	1.391(6)
C23–C24	1.367(9)	1.376(5)	1.377(6)
C24–C25	1.375(9)	1.389(5)	1.381(6)
C25–C26	1.378(9)	1.378(4)	1.382(6)
C27–C28		1.503(4)	1.524(6)
C28–C31A			1.469(10)
C28–C30B			1.479(12)
C28–C29A			1.482(11)
C28–C29B			1.501(12)
C28–C31B			1.565(12)
C28–C30A			1.626(12)
C33–C34			1.654(11)

[a] To allow comparison with **H_4L**, the atom labels of **2** and **3** have been renumbered compared to the CIF files already published.[22]

Table 3 Bond distances (Å) and angles (°) around the Zn ions in $[\{Zn_2(IPCPMP)(OAc)\}_2](PF_6)_2$ (**2**) and $[\{Zn_2(IPCPMP)(Piv)\}_2](PF_6)_2$ (**3**)

	2[a]	**3**[a]
Zn1–N1	2.112(2)	2.087(3)
Zn1–N2	2.1736(19)	2.221(3)
Zn1–O1	2.0394(17)	2.022(3)
Zn1–O3	1.9680(16)	1.956(3)
Zn1–O5	1.9860(17)	2.006(3)
Zn2–N3	2.1132(19)	2.102(3)
Zn2–N4	2.111(2)	2.147(3)
Zn2–O2	2.0543(17)	1.990(3)
Zn2–O3	2.0246(16)	2.004(2)
Zn2–O4	2.0741(17)	2.069(3)
Zn1–Zn2[b]	3.4019(4)	3.3949(6)
Zn1–Zn1[b]	4.9326(4)	5.1398(7)
Zn1–Zn2i[b]	4.7630(4)	4.9327(6)
Zn1–O3–Zn2	116.86(8)	118.02(13)
N1–Zn1–N2	77.78(8)	77.81(13)
O1–Zn1–N1	115.31(7)	114.95(12)
O1–Zn1–N2	80.15(7)	79.55(11)
O3–Zn1–N1	119.90(7)	122.24(12)
O3–Zn1–N2	92.28(7)	89.96(11)
O3–Zn1–O1	121.01(7)	117.80(11)
O3–Zn1–O5	100.63(7)	100.99(11)
O5–Zn1–N1	94.92(8)	94.94(13)
O5–Zn1–N2	167.07(8)	168.96(11)
O5–Zn1–O1	93.67(7)	96.32(11)
N3–Zn2–N4	81.24(8)	81.30(12)
O2–Zn2–N3	115.42(7)	122.30(11)
O2–Zn2–N4	93.27(7)	97.04(12)
O2–Zn2–O3	146.06(7)	138.36(11)
O2–Zn2–O4	84.47(7)	86.17(12)
O3–Zn2–N3	98.50(7)	99.32(11)
O3–Zn2–N4	90.88(7)	90.08(11)
O3–Zn2–O4	89.96(7)	89.11(11)
O4–Zn2–N3	101.44(7)	94.95(12)
O4–Zn2–N4	177.04(7)	175.98(12)

[a] To allow comparison with H_4L, the atom labels of **2** and **3** have been renumbered compared to the CIF files already published.[22] [b] Determined using Diamond v3.1 (www.crystalimpact.com/diamond/).

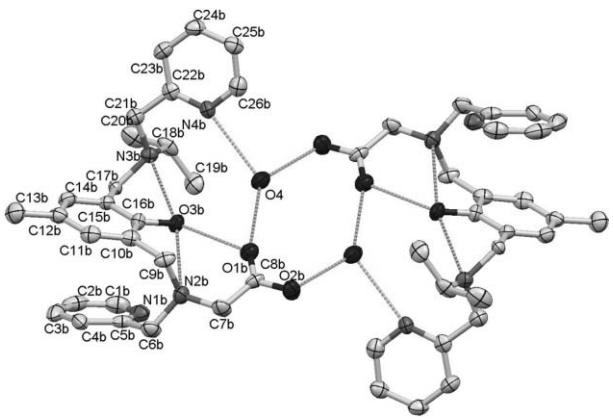

Fig. 4 Mercury[72] plot of $H_4IPCPMP(PF_6)_2{\cdot}H_2O$ ($\mathbf{H_4L}$). Counter-ions have been omitted for clarity and ellipsoids are drawn at 50% probability.

prone than **3** to dissociate into two dinuclear complexes in solution. Both exogenous carboxylates (the acetate and the pivalate) bridge in an unsymmetrical *syn*,*syn*-μ-1,3 manner with shorter bonds to Zn1 (**2**: Zn1–O5 1.9860(17), Zn2–O4 2.0741(17) Å and **3**: Zn1–O5 2.006(3), Zn2–O4 2.069(3) Å). The phenolate is also unsymmetrically bridging with shorter bonds to Zn1 (**2**: Zn1–

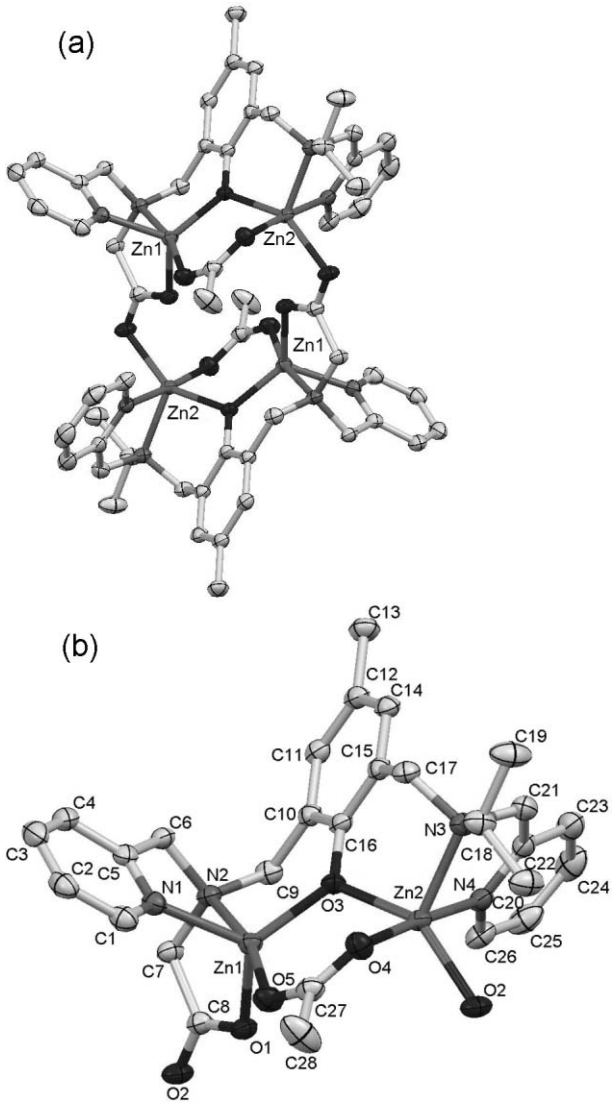

Fig. 5 MERCURY[72] plots of the dimeric structure of $[\{Zn_2IPCPMP(OAc)\}_2]^{2+}$ **2** (a) and one of the dinuclear entities (**2***) of the dimer (b). Solvent and counterions have been omitted for clarity and the ellipsoids are drawn at 50% probability. To allow comparison with $\mathbf{H_4L}$, the atom labels of **2** and **3** have been renumbered compared to the CIF files already published.[22]

O3 1.96880(16), Zn2–O3 2.0246(16) Å and **3**: Zn1–O3 1.956(3), Zn2–O3 2.004 Å). The only bonds that are longer to Zn1 than Zn2 are those from the tertiary amines (**2**: Zn1–N2 2.1736(19), Zn2–N3 2.1132(19) Å and for **3**: Zn1–N2 2.221(3), Zn2–N4 2.147(3) Å). Que and coworkers[31] have argued that such elongation of metal–tertiary amine bonds may be due to strain imposed by coordination of the chelating arms of the ligand. In the case of the unsymmetric ligand IPCPMP, Zn1 is involved in three coordination rings (compared to two for Zn2). In agreement with the above-mentioned argument regarding strain, the tertiary amine (N2) bound to Zn1 is further away from the metal than that bound to Zn2 (N3), where only two coordination rings exist. The resulting weaker interaction between N2 and Zn1 might also explain the shorter bonds to the other groups from Zn1 relative to Zn2 and hence the unsymmetrical bridging.

Despite the unsymmetrical coordination of the bridging carboxylates, the two C–O bonds in each bridging carboxylate moiety have similar bond distances (**2**: O1–C8 1.262(3), O2–C8 1.250(3), O4–C27 (1.259(3), O–5C27 (1.259(3) Å and **3**: O1–C8 1.265(5), O2–C8 1.247(5), O4–C27 (1.250(5), O5–C27 (1.265(5) Å). This observation is consistent with the delocalized nature of the C=O bond and in contrast with what is observed for the protonated carboxylates in the structure of **H_4L**, where the corresponding distances are significantly different (O1–C8 1.232(7), O2–C8 1.310(7) Å). Although pivalate is a slightly stronger base, and hence a stronger donor, the difference in pK_a is not large (pK_a(HPiv) = 5.03; pK_a(HOAc) = 4.76) and the oxygen to zinc distances (*vide supra*) for the two different carboxylate bridges are fairly similar for **2** and **3**. The bonds *trans* to these donors are however slightly longer for **3** (Zn1–N2 2.221(3), Zn2–N4 2.147(3) Å) than for **2** (Zn1–N2 2.1736(19), Zn2–N4 2.111(2) Å). The three metal–metal distances in the tetranuclear structure of **2** are Zn1–Zn2 3.4019(4) Å, Zn1–Zn2^i 4.7630(4) Å and Zn1–Zn1^i 4.9326(4) Å which may be compared to the corresponding distances in **3**, *i.e.* Zn1–Zn2 3.3949(6) Å, Zn1–Zn2^i 4.9327(6) Å and Zn1–Zn1^i 5.1398(7) Å. The distances found in the trinuclear active sites discussed above (Fig. 1) are: alkaline phosphatase (3.9, 4.9 and 7.1 Å), nuclease P1 (3.2, 4.7, 5.8 Å) and phospholipase C (3.3, 4.7, 6.0 Å). Furthermore, the distances between Zn1 and Zn2 in **2** and **3** are similar to those in the closely related tetranuclear Zn complex $[\{Zn_2(ICIMP)(O_2CCHPh_2)\}_2]^{2+}$ (Zn1–Zn2 3.459(1) Å)[24] where diphenylacetate acts as exogenous carboxylate. The trend with unsymmetrical bridges carries over to this complex but the imidazole groups, that are stronger σ-donors, have shorter bonds to the Zn ions than the corresponding pyridyl groups in **2** and **3**.

Comparing the structures of the coordinated and non-coordinated IPCPMP ligand, there is little change in the distances and angles in the carbon backbone of the ligand upon coordination, with the exception of the C–C bond between the carbonyl carbon (C8) and the α-carbon (C7), where the distance increases significantly (**H_4L**: 1.477(8) Å, **2**: 1.520(3) Å and **3**: 1.521(5) Å). This change indicates that significant strain is introduced upon coordination of Zn. The only other notable change is that mentioned above for the C–O bonds of the carboxylates, that become more symmetric when bridging between two metals than when protonated and hydrogen-bonded to other heteroatoms. These differences are well illustrated by the IR spectra of the ligand compared to that of the complex (*vide infra*).

IR spectroscopy

Due to the characteristic signatures of carboxylate functionalities in infrared spectroscopy, FTIR was used to study **H_4L** (H_4IPCPMP$(PF_6)_2$), **2** and **3** in the solid state as KBr pellets, and **2** in various solutions. The antisymmetric and symmetric stretches for the carboxylic acid group in **H_4L** occur at 1710 and 1229 cm^{-1}, respectively, whereas in **2** and **3** they are shifted to about 1600 and 1420 cm^{-1}, as is usually observed upon coordination of a carboxylate group. This change correlates well with the observed change in carboxylate bond lengths upon coordination (*vide supra*). The FTIR spectra of **2** and **3** in KBr are very similar except that the peaks for **3** are broader and less well defined. The spectrum of **2** correlates very well with the solid state structure. There are two peaks at 1609 and 1600 cm^{-1} (ν_2 and ν_3 in Fig. 6(a)) that can be assigned to antisymmetric carboxylate stretches (for **3** these are unresolved, *cf.* experimental section) and the corresponding symmetric stretches are assigned to resonances at 1436 and 1414 cm^{-1} (ν_5 and ν_6). The peak at 1485 cm^{-1} (ν_4) and the cluster of peaks with intermediate intensity around 1570 cm^{-1} (not labelled) are assigned to aromatic C=C stretches. The difference ($\Delta\nu$) between the symmetric (ν_{sym}) and antisymmetric (ν_{asym}) carboxylate stretches is often used to infer the type of coordination to the metal. A $\Delta\nu > 200$ is usually taken to indicate monodentate coordination to the metal while $\Delta\nu < 200$ indicates bridging and/or chelating coordination if an ionic carboxylate salt can be ruled out.[32] For **2** in KBr, the differences are either 173 and 186 cm^{-1} ($\nu_2 - \nu_5$ and $\nu_3 - \nu_6$) or 164 and 195 cm^{-1} ($\nu_2 - \nu_6$ and $\nu_3 - \nu_5$) for the carboxylate resonance depending on the assignment of the symmetric and antisymmetric stretches for each carboxylate. As discussed below, the former assignment is more reasonable.

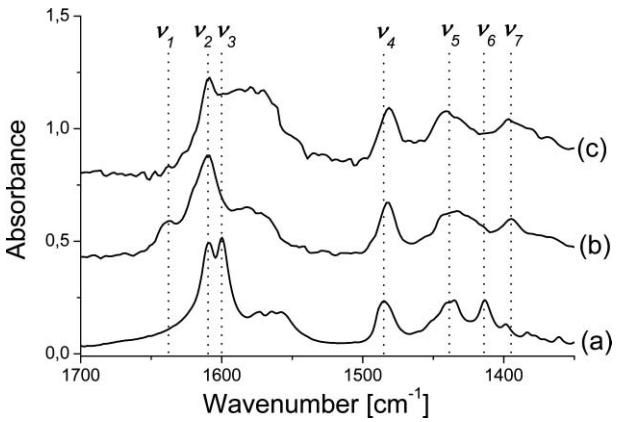

Fig. 6 FTIR spectra of $[\{Zn_2IPCPMP(OAc)\}_2]^{2+}$ **2** in KBr (a), acetonitrile (b) and a mixture of acetonitrile and water 1 : 1 (v/v) (c).

Complex **2** is readily soluble in acetonitrile, and upon dissolution to a concentration of 25 mM (w.r.t. $[\{Zn_2(IPCPMP)(OAc)\}_2][PF_6]_2$) the FTIR spectrum changes to that in Fig. 6(b). In acetonitrile solution, the resonances at ν_3 and ν_6 are absent and have been replaced by resonances at 1638 (ν_1) and 1395 cm^{-1} (ν_7). These new bands correspond well to a monodentate carboxylate group with $\Delta\nu = 243$ cm^{-1}, suggesting that the tetranuclear complex dissociates into two dinuclear entities (**2***) in this solvent. The dinuclear zinc complex **2*** is likely to retain its structure (*cf.* Fig. 5(b)). This observation supports the assignment mentioned above, (*i.e.* $\nu_2 - \nu_5$ represents one carboxylate, and $\nu_3 - \nu_6$ the other).

For solubility reasons, *i.e.* compatibility between substrate and Zn complex, and in order to be able to compare the present results with related studies,[33–40] the reactivity studies were performed in a 1 : 1 acetonitrile–water mixture. Therefore this solvent combination was also studied by FTIR (Fig. 6(c)). The analysis becomes much more difficult, however, as water can form hydrogen bonds to the oxygen atom(s) of the carboxylate moieties, forming pseudo-bridged systems.[32] This would explain the disappearance of the ν_1 resonance and possibly the formation of the strong but broad and poorly defined peaks around 1590 cm^{-1}. Due to the rather broad and undefined features of the spectrum of **2** in acetonitrile–water no further conclusions can be drawn.

Table 4 Calculated overall stability constants (logβ) and derived stepwise dissociation constants (pK) for the proton and Zn^{2+} complexes of L (IPCPMP) at 25 °C with $I = 0.2$ M (KCl)

Equilibrium processes	logβ	pK_a
$L^{2-} + H^+ = HL^-$	9.28 (1)	9.28
$L^{2-} + 2H^+ = H_2L$	14.71(1)	5.43
$L^{2-} + 3H^+ = H_3L^+$	17.12(2)	2.41
$L^{2-} + 4H^+ = H_4L^{2+}$	18.75(2)	1.63
$Zn^{2+} + L^{2-} = [ZnL]$	11.2(1)	
$2Zn^{2+} + L^{2-} = [Zn_2L]^{2+}$	15.25(2)	
$2Zn^{2+} + L^{2-} + H_2O = [Zn_2L(OH)]^+ + H^+$	8.38(6)[a]	
$2Zn^{2+} + L^{2-} + 2H_2O = [Zn_2L(OH)_2] + 2\ H^+$	1.67(3)	
$[Zn_2L]^{2+} + 2H_2O = [Zn_2L(OH)_2]^+ + 2H^+$		13.58
$[Zn_2L]^{2+} + H_2O = [Zn_2L(OH)]^+ + H^+$		6.87[b]
$[Zn_2L(OH)]^+ + H_2O = [Zn_2L(OH)_2] + H^+$		6.71[c]

[a] Due to the cooperativity of the deprotonation of two water molecules, the formation of the dihydroxo species is favoured in this system, while the presence of the monohydroxo species is almost negligible. [b] The pK value refers to the first dissociation process of a coordinated water in the dinuclear complex. [c] The pK value refers to the second dissociation process of a coordinated water in the dinuclear complex.

Coordination in aqueous solution

To further study the species distribution in aqueous solution, a potentiometric titration with $H_4IPCPMP(PF_6)_2$ (**H_4L**) and $ZnCl_2$ was performed. The determined stability constants are shown in Table 4 along with the calculated acid dissociation constants (pK_a) for the stepwise deprotonation processes. The titration curves are shown in the ESI (Fig. S2).† First, the acid dissociation constants of the ligand were determined. As seen in the species distribution diagram in Fig. 7(a), formation of **H_4L** only occurs at very low pH and all basic positions are not protonated within the pH range of this study. The first proton of $[H_4IPCPMP]^{2+}$ is completely released at about pH 3, most probably from the carboxylic acid moiety. The next two deprotonation steps are likely to occur at the two ammonium groups; the large difference between these two pK_a values may be due to different degrees of hydrogen bonding to nearby functional groups. The fairly low pK_a values may also be related to hydrogen bonding to the phenolic proton which makes further protonation of the amine to form the ammonium cation less favourable, thus giving a large K_a for the deprotonation of the ammonium moiety.[41]

Fitting of the data from potentiometric titrations of 1 : 1 and 2 : 1 mixtures of Zn^{2+} and 1.2 mM $H_4IPCPMP(PF_6)_2$ (**H_4L**) resulted in the calculated stability constants listed in Table 4. Species distributions are depicted in Fig. 7(b) and (c), respectively. When one equivalent of Zn^{2+} is added, a mononuclear species ([ZnL]) is the most prevalent species over a very large pH range. Deprotonation of metal bound water only occurs at very high pH and then only with the simultaneous formation of a dinuclear species ($[Zn_2L(OH)_2]$). This observation indicates that in the mononuclear complex [ZnL], the zinc ion is coordinated in the tetradentate pocket of the ligand that contains the carboxylate donor, since the highly anionic environment is expected to make deprotonation of coordinated water molecules less favourable. It is not possible to determine the exact pK_a value of this process on the basis of the pH range used for the potentiometric studies but these studies indicate that the value is higher than 9. Regarding the preferred coordination site of the zinc ion, we have found that the preparation of a mononuclear Fe(III) complex of

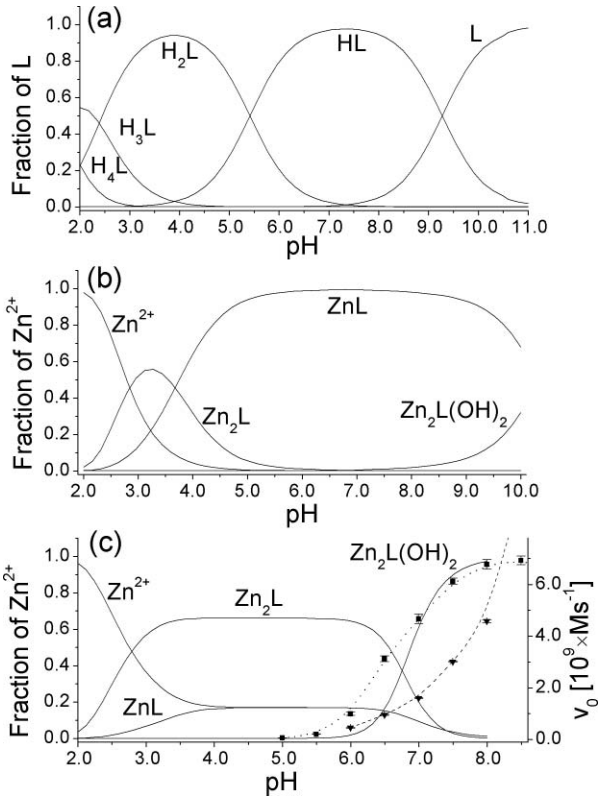

Fig. 7 (a) Species distribution curves for IPCPMP (L). (b) For 1 : 1 Zn^{2+} : IPCPMP and (c) 2 : 1 Zn^{2+} : IPCPMP. $C_{ligand} = 1.2 \times 10^{-3}$ M. In (c) are also included the pH dependence of the initial rates for the cleavage of BDNPP (···●···) and HPNP (---▲---).

($H_4IPCPMP(PF_6)_2$ leads exclusively to coordination of the ferric ion in the tetradentate pocket.[42] A surprising feature is the high stability of the mononuclear species in relation to the corresponding dinuclear one when two equivalents of Zn^{2+} are used. In the pH range 3.5–6.5, the ratio of dinuclear *vs.* mononuclear complex is about 3 : 1 and a large fraction (~20%) of the Zn^{2+} remains non-coordinated up to just above pH 6. This can be explained by the very different coordinating abilities of the two side arms of the IPCPMP ligand. The chelate effect of the tridentate pocket is less than that for the tetradentate pocket, and it is likely that the metal affinity of the tridentate pocket at low to intermediate pH is significantly less than that of the tetradentate pocket. A similar behaviour was found for *N*,*N*′-bis(5-methyl-imidazole-4-ylmethyl)-1,3-diaminopropan-2-ol (bimido) which only has two coordinating groups on either side of the alcohol groups.[43] In the case of bimido, it was found that only a mononuclear complex was stable between pH 4.5–7 in the presence of two equivalents of zinc; this observation could be explained by a crystal structure of this species, revealing a non-coordinated alcohol group and coordination of the single zinc ion by all the other groups in the ligand. A similar phenomenon is unlikely to occur in the present case due to the rigidity of the phenol linker of IPCPMP (L). It is also interesting to note that the stoichiometry upon deprotonation of the metal-coordinated water molecules implies the formation of two hydroxido groups ($[ZnL(OH)_2]$) with an overall stability constant logβ = 1.67(3). This process can be separated into two deprotonation steps having close to identical

pK_a values of 6.87 and 6.71, as calculated from the corresponding stability constants in Table 4. Values as low as this for the protolysis of coordinated water at Zn^{2+} is often taken as evidence for the formation of bridging hydroxido groups between the two zinc ions,[44–46] suggesting that $[Zn_2L(OH)_2]$ has the structure depicted in Fig. 8(a). There are however mononuclear zinc complexes that have been reported to have aqua ligands with pK_a < 7 although they include highly specialized bulky ligands with hydrophobic metal compartments and the actual species is not always clearly identified.[21,46–48] As noted by Buchholz *et al.*[49] a strict correlation between pK_a and terminally or bridging coordination mode of the water molecule is difficult to find. Furthermore, it is difficult to rationalize the close to identical pK_a values for the formation of these two bridges since the first deprotonation should influence the second considerably.

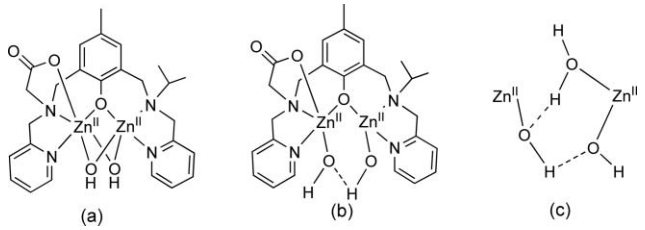

Fig. 8 Proposed structures of the species $[Zn_2L(OH)_2]$ identified in the potentiometric studies with two bridging (a) or two terminal but hydrogen bonded (b) hydroxido groups. In (c) a third proposal displaying hydrogen bonding between two terminal hydroxides and a coordinated water molecule is shown.

The very similar values for the deprotonation constants (pK_a 6.87 and 6.73) may suggest a cooperative effect where the deprotonation of one water on one Zn favours the deprotonation of the second water molecule (on the other Zn ion) through hydrogen bonding (Fig. 8(b)). Low pK_a values in the range of 7–8 have been found for diaqua species with a hydrogen bonded Zn–OH $\cdots$ H_2O–Zn structure, but then only deprotonation of one of the water molecules was detected.[50,51] This O_2H_3 unit was favoured for metal–metal distances >4 Å, larger than that in **2**.[52] If this type of hydrogen bonding motif is responsible for the low pK_a of the coordinated water molecules, involvement of a third water molecule to stabilize the two hydroxides in an O_3H_4 unit may explain the observed behaviour (Fig. 8(c)). When two equivalents of Zn^{2+} were used, precipitation was observed at pH > 8. Titrations using 1.5 equivalents do not have this problem and the resultant curve gives no indication of further deprotonation of metal-coordinated water even though there should still be one site available for water coordination due to the non-coordinating isopropyl group. Probably the highly negative charge contributed by four anionic coordinating groups makes further metal hydrolysis in $[Zn_2L(OH)_2]$ unfavourable.

The existence of the mononuclear and dinuclear complexes discussed above is indirectly supported by ESI-MS experiments of a 2 : 1 solution of $ZnCl_2$–H_4IPCPMP$(PF_6)_2$ at pH 7.8, which show peaks for the species $[ZnL]^+$, $[Zn_2LCl]^+$ and $[Zn_2L(OH)Cl]K$, but no species corresponding to $[Zn_2L(OH)_2]$ could be observed (see ESI, Fig. S2†). In an effort to detect $[Zn_2L(OH)_2]$ under conditions that are similar to those used in the reactivity studies (*vide infra*), ESI-measurements of buffered solutions of $[\{Zn_2(IPCPMP)(OAc)\}_2][PF_6]_2$ (**2**) were made but no peaks could be discerned due to the large buffer-derived peaks that obscure all other peaks. However, when ESI spectra of **2** were recorded in water–MeOH (1 : 1 v/v) solutions, where the pH was adjusted by addition of dilute NaOH, a peak attributable to $[Zn_2L(OH)_2]$ ($[Zn_2(IPCPMP)(O)(OH)]$, $[Zn_2(IPCPMP)(O)_2]$) could be detected at 611 (±0.6) amu at pH 7.0 and 7.5, along with a more intense peak at 595 amu attributable to $[Zn_2L(OH)]$ ($[Zn_2(IPCPMP)(O)]$), as well as a peak envelope for $[Zn_2(IPCPMP)(OAc)]$ (Fig. S4, ESI†).

Reactivity studies

The reactivity of **2** towards hydrolysis of phosphate diesters was investigated using 2,4-bis-dinitrophenol-phosphate (BDNPP, Scheme 1) as a substrate. The initial rates were measured by following the absorbance of the formed 2,4-nitrophenolate (pK_a = 4.07, ε = 12 100 M^{-1} cm^{-1}) at 400 nm in buffered water–acetonitrile 1 : 1 (v/v) solution with 0.1 M $NaClO_4$ concentration in order to maintain ionic strength. The pH dependence of the reactivity is displayed in Fig. 9 along with that previously determined for the transesterification of the substrate 2-hydroxypropyl-4-nitrophenol phosphate (HPNP).[22] For BDNPP, the initial rates show a sigmoidal dependence on the pH, reaching a modest maximum rate 127 times faster than that of the non-catalyzed reaction (at pH 7.5). The change to zero order with respect to hydroxide concentration at pH > 7.5 clearly indicates that a pre-equilibrium process involving deprotonation of a functional group is important for reactivity. The pK_a of this process has been estimated to 6.63(5) by fitting a sigmoidal Boltzmann function to the data. The curve also follows the formation of the hydroxido species $[Zn_2L(OH)_2]$ (Fig. 7(c)) as determined by the potentiometric studies, and the calculated pK_a values agree well with those determined from the kinetic measurements. This indicates that the active species is $[Zn_2L(OH)_2]$, or possibly $[Zn_2L(OH)]$ since this species forms to some extent at the same pH and may be favoured when a bridging acetate or substrate is present. Another possibility is that the active species, which binds and activates the substrate, is $[Zn_2L]$ (or possibly [ZnL]) and that the substrate is attacked by a non-coordinating hydroxide. Morrow and co-workers[53] have shown that a dinuclear Zn(II) complex of the ligand 1,3-bis(1,4,7-triazacyclonon-1-yl)-2-hydroxypropane is more strongly inhibited

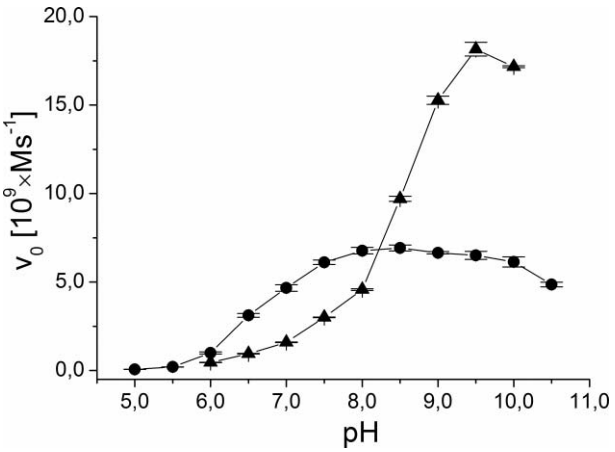

Fig. 9 Graphs displaying the pH dependence of the hydrolysis of BDNPP (●) and the transesterification of HPNP(▲) catalyzed by **2**.

at pH lower than that for maximal rate. If a similar situation were to occur in the present system, the maximum rate reached at about pH 8 is then a result of the balance between a decrease in reactivity due to decreasing concentration of $[Zn_2L]$ and increase in reactivity due to increasing hydroxide concentration.

It is interesting to note that the transesterification of HPNP (a RNA mimic, Scheme 1) does not follow the pH dependence observed for BDNPP. Although the curve still is sigmoidal, the rate increment starts at much higher pH and thus does not appear to be associated with the formation of the deprotonated species $[Zn_2L(OH)_2]$ (Fig. 7(c)). The maximum rate that is reached at about pH 9.5 could be a result of a pre-equilibrium deprotonation of the hydroxyl moiety of the substrate. Metal coordination of this hydroxyl moiety is necessary in order to induce a sufficiently low pK_a value to achieve complete protolysis at pH 9.5–10. A pK_a of 12.8 has been determined for a non-coordinated 2′-hydroxyl group of an analogue to HPNP that contains a ribose unit and an ethyl group on the phosphate.[54] The difference in pK_a for non-coordinated HPNP is expected to be small and a lowering of 3–4 units upon coordination could be feasible considering that water coordinated to hydrated Zn(II) reduces its pK_a to 9.6.[55] For both substrates, a decline in activity is observed at high pH (10–10.5); this decline may be associated with decomposition of the zinc complex, and such decomposition may also cause or add to the observed pH dependence for HPNP transesterification.

The dependence of the initial rate on complex and substrate concentration was studied in order to further elucidate the reactivity. As shown in Fig. 10(a), there is a strict first order dependence of the initial rate on the catalyst concentration for both HPNP and BDNPP and second order rate constants of $k_{2nd,HPNP} = 0.032(3)\ M^{-1}\ s^{-1}$ and $k_{2nd,BDNPP} = 0.034(1)\ M^{-1}\ s^{-1}$ could be calculated from the slope and the substrate concentration, assuming that the latter is constant for initial rate conditions. Here, the concentration is given for the assumed dinuclear complex (**2***) that will form upon dissociation of the tetranuclear dimer. Fig. 10(b) shows saturation kinetics for the substrate dependence indicating binding of the substrate in a pre-equilibrium step. This data could be fitted to the Michaelis–Menten equation (eqn (1)) yielding values for K_m and V_{max} that are reported in Table 5 and used to calculate other parameters.

$$v_0 = \frac{V_{max}[S]}{K_m + [S]} \quad (1)$$

The K_M values indicate that the complex binds HPNP more strongly than BDNPP (3.6 and 16 mM respectively), possibly due to the more electron rich nature of the phosphate moiety in HPNP. However, involvement of the 2-hydroxyl group in the coordination of the HPNP cannot be excluded. The binding of HPNP is stronger than for several other similar dinuclear

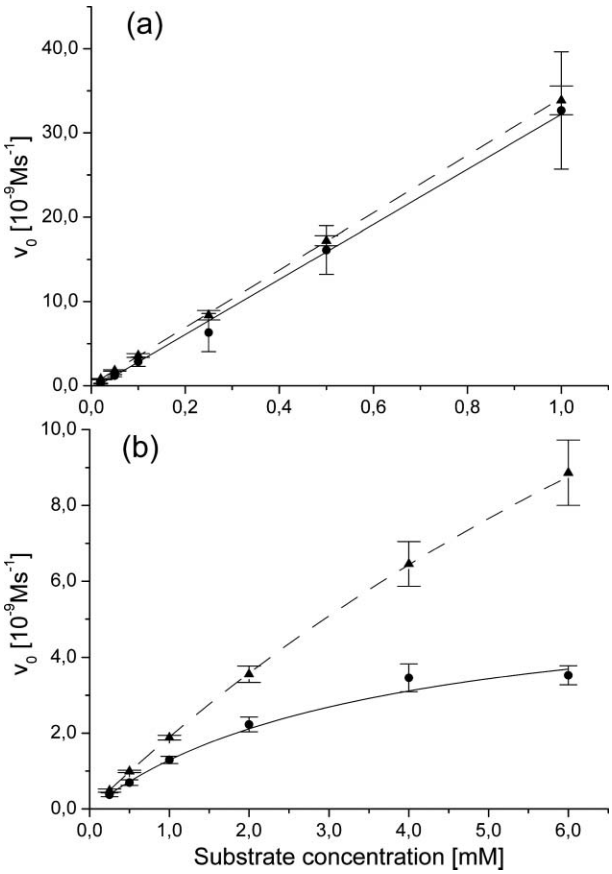

Fig. 10 The dependence on concentrations of complex (a) and substrate (b) for the transesterification of HPNP (●) and the hydrolysis of BDNPP (▲) catalyzed by **2**. In (a) the complex concentration is given for the dinuclear entity **2*** and [BDNPP] = 1.0 mM. In (b) $[2^*] = 5.0 \times 10^{-5}$ M.

Zn complexes from symmetric ligands containing alkoxide or phenolate groups as bridges (K_M = 5.4–16 mM),[43,44,56,57] while a calix[4]arene based complex displays much stronger binding (K_M = 0.018 mM).[58] The k_{cat} for HPNP transesterification enhanced by **2** ($1.2 \times 10^{-4}\ s^{-1}$) is however significantly lower compared to all of these complexes (6.4×10^{-4}–$0.01\ s^{-1}$)[43,44,56–58] and this is 560 times (k_{cat}/k_{uncat}) that of the uncatalyzed reaction ($k_{uncat} = 2.13 \times 10^{-7}\ s^{-1}$ at pH 8.5)[33] and an overall efficiency (k_{cat}/K_M) of 0.033 $M^{-1}\ s^{-1}$.

The k_{cat} for BDNPP hydrolysis was calculated to $6.4 \times 10^{-4}\ s^{-1}$ and due to the weak binding the efficiency of the complex to promote BDNPP hydrolysis is quite low ($k_{cat}/K_m = 0.040\ M^{-1}\ s^{-1}$) but there is still a 2×10^4 fold rate acceleration (k_{cat}/k_{uncat}) compared to the uncatalyzed reaction ($k_{uncat} = 3.2 \times 10^{-8}\ s^{-1}$ in water–acetonitrile 1 : 1 (v/v);[59] previous studies on BDNPP hydrolysis[34–40] in this solvent mixture have used a k_{uncat} value for solutions with

Table 5 Second order rate constants and kinetic parameters from the fitting of the Michaelis–Menten equation to the dependence of substrate concentration for the transesterification of HPNP and the hydrolysis of BDNPP at pH 8.5

	k_{2nd}[a]	$V_{max}/10^{-9}$ M s^{-1}[b]	K_M/mM[b]	K_{ass}/M^{-1}[c]	$k_{cat}/10^{-4}\ s^{-1}$[d]	$k_{cat}/K_M/M^{-1}\ s^{-1}$	k_{cat}/k_{uncat} [10^4]
BDNPP	0.034(1)	32(10)	16(5)	64	6.4	0.040	2.0
HPNP	0.032(3)	5.9(7)	3.6(6)	280	1.2	0.033	0.056

[a] Second order rate constant defined by $v_0 = k_{2nd}[2^*][Sub]$ where [Sub] is the substrate concentration. [b] The standard errors from the non-linear curve fitting are given within parentheses. [c] $K_{ass} = 1/K_M$ [d] $k_{cat} = V_{max}/[2^*]$

only water (1.8×10^{-7} s^{-1}) and for **2** this would yield $k_{cat}/k_{uncat} = 3.8 \times 10^3$).

To our knowledge, only a few studies on hydrolysis of BDNPP by zinc complexes have been reported and only pseudo-first order rate constants with the complexes in excess were calculated so no straightforward comparison can be made here.[60–63] Neves and coworkers[34–40] have tested several heterodinuclear complexes for activity towards BDNPP cleavage. The pH optima of these complexes and **2** differ, but a comparison of k_{cat} at respective pH optimum makes it clear that **2** rivals the heterodinuclear complexes with respect to k_{cat} although it binds the substrate much more weakly and hence suffers from lower overall efficiency (k_{cat}/K_M 0.0398 M^{-1} s^{-1} (**2**) *vs.* 0.075–0.16 M^{-1} s^{-1}).[34–40] The catalytic efficiency is also low when compared to the dinuclear nickel complex of 2-[*N*-(2-(pyridyl-2-yl)ethyl)(1-methylimidazol-2-yl)aminomethyl]-4-methyl-6-[*N*-(2-(imidazol-4-yl)ethyl)amino methyl]phenol),[64] which has been reported to have a k_{cat}/K_M value of 68 M^{-1} s^{-1}, and displays both rapid turnover ($k_{cat} = 0.386$ s^{-1}) and tight substrate binding ($K_M = 5.67$ mM).

Conclusions

In the present work, the complete synthesis and structural characterization of the unsymmetrical dinucleating ligand IPCPMP has been presented and its ability to coordinate Zn(II) has been studied. In the solid state, two tetranuclear complexes have been structurally characterized but both IR spectroscopy and mass spectra indicate that the tetranuclear complex $[\{Zn_2IPCPMP(OAc)\}_2][PF_6]_2$ (**2**) dissociates into two dinuclear entities when dissolved in acetonitrile or an acetonitrile–water mixture. A zinc complex of the unsymmetrical ligand has been shown to be a better promoter of the transesterification of HPNP (an RNA mimic) than a similar but symmetric ligand (BCPMP), probably due to lower coordination number on one of the Zn(II) ions in the IPCPMP case.[22] The pH dependence of the activity suggests that the hydroxyl group of the HPNP is activated by coordination and is deprotonated before its nucleophilic attack on the phosphorus center (Scheme 3(a)). The mode of coordination of the phosphate moiety has not been determined. A detailed investigation of the reactivity of $[\{Zn_2IPCPMP(OAc)\}_2][PF_6]_2$ (**2**) towards the hydrolysis of BDNPP (a DNA mimic) has been undertaken and the pH dependence indicates that a metal-bound water molecule needs to be deprotonated for activity. Potentiometric titration studies indicate that a terminally bound hydroxide is the active nucleophile, and weak binding of the substrate in an pre-equilibrium step leads us to propose a mechanism in agreement with Scheme 3(b), where the substrate binds in a monodentate fashion to Zn2 before being attacked by the nucleophile coordinated to Zn1. The ligand IPCPMP has recently been shown to be able to form heterodinuclear complexes with various metals[65] and further investigations are being directed toward studying the effect of metal substitution on the above phosphoryl transfer reactions.

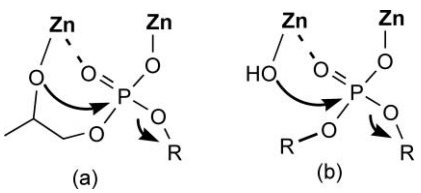

Scheme 3 Proposals for the nucleophilic attack in the cleavage of (a) HPNP and (b) BDNPP catalyzed by the proposed active species formed from $[\{Zn_2(IPCPMP)(OAc)\}_2][PF_6]_2$

Experimental

Materials

All solvents were of at least 99.5% purity and used as received or dried either by distillation from CaH_2 (methanol, 2-propanol) or by keeping over molecular sieves in a sealed bottle over night (acetone 3 Å molecular sieves, dichloromethane 4 Å molecular sieves). Reagents were of at least 99% purity, obtained from commercial sources and used as received. The starting materials *N*-(ethoxycarbonylmethyl)-*N*-((2-pyridylmethyl)amine (**b**),[66] 2-(hydroxymethyl)-6-carbaldehyde-4-methyl-phenol[25] (**c**), the barium salt of 2-hydroxypropyl-*p*-phenylphosphate[67] and the sodium salt of bis(2,4-nitrophenyl)phosphate[59,68] were synthesized according to literature procedures.

Physical measurements

UV-vis spectroscopy and kinetic measurements were performed on a Varian 300 Bio UV/vis spectrophotometer equipped with a 12-position thermostated cell changer. Infrared spectra were collected on a Nicolet Avatar 360 FTIR spectrometer for solid KBr discs and a Digilab Excalibur FTIR spectrometer equipped with an Axiom Analytical DPR-210 dipper system and a MCT detector for liquid samples. Fast atom bombardment (FAB+) and high resolution mass spectra were measured on a JEOL SX-102 instrument. NMR spectroscopy was performed on a Varian Inova 500 spectrophotometer in $CDCl_3$ solution unless noted otherwise and referenced to the residual proton signal of the solvent.

Syntheses

***N*-isopropyl-*N*-(2-pyridylmethyl)amine (a).** A total of 4.50 ml (0.0420 mmol) pyridyl carboxaldehyde was dissolved in 200 ml dichloromethane and 8.0 ml (93 mmol) isopropyl amine was added. The mixture was stirred at room temperature for 10 min before adding 20.7 g (0.0977 mmol) of sodium tris(acetoxy)borohydride and the solution was left stirring at room temperature for 16 h after which the reaction was complete according to TLC (heptane : ethyl acetate : triethylamine 2 : 1 : 1). The reaction mixture was washed with 3 × 150 ml saturated Na_2CO_3(aq) and the water phases were extracted with 3 × 50 ml dichloromethane. The combined organic phases were dried over Na_2SO_4(s), filtered and evaporated to yield 6.24 g (98.8%) of a yellowish oil that was pure according to NMR. ^{1}H NMR (500 MHz) $CDCl_3$: δ 8.54 (d 1H), 7.61 (t 1H), 7.28 (d 1H), 7.13 (t 1H), 3.88 (s 2H), 2.85 (sept. 1H), 1.81 (s (br), 1H), 1.10 (d 6H).

2-(*N*-isopropyl-*N*-(2-pyridylmethyl)amino-methyl-6-hydroxy-methyl-4-methylphenol (d). A total of 5.019 g (0.03002 mol) of 2-(hydroxymethyl)-6-carbaldehyde-4-methyl-phenol and 3.276 g (0.0218 mmol) of (**a**) was dissolved in 80 ml of dichloromethane under an inert atmosphere in a dry round-bottom flask with 4 g of 4 Å molecular sieves to remove water formed in the

reaction. After stirring at room temperature for 45 min, 14.0 g of sodium tris(acetoxy)borohydride was added. After 3 h of stirring at room temperature, the reaction was complete according to TLC (chloroform : heptane 3 : 1 with NH_3 extracted from 25% aqueous ammonia) and was quenched by addition of 100 ml of saturated $NaHCO_3$(aq). The pH was adjusted to 8 with saturated Na_2CO_3(aq). The organic phase was further washed two times with saturated Na_2CO_3 before drying over Na_2SO_4(s), filtering and removal of solvent under vacuum. The crude product was purified by column chromatography on silica using $CHCl_3$ with 2% methanol as eluent yielding 4.81 g (73.3%). ^{1}H NMR (500 MHz) $CDCl_3$: δ 8.55 (ddd, 1H, $J = 0.9$ Hz, $J = 1.8$ Hz, $J = 4.9$ Hz) 7.66 (dt, 1H, $J = 1.8$ Hz, $J = 7.7$ Hz) 7.33 (d, 1H, $J = 7.8$ Hz) 7.18 (ddd, 1H, $J = 1.0$ Hz, $J = 4.9$ Hz, $J = 7.5$ Hz) 6.91 (d, 1H, $J = 1.6$ Hz) 6.75 (d, 1H, $J = 1.5$ Hz) 3.12 (td, 1H, $J = 6.5$ Hz, $J = 13.1$ Hz).

2-(*N*-isopropyl-*N*-((2-pyridyl)methyl)aminomethyl)-6-(*N*-(ethoxycarbonylmethyl)-*N*-((2-pyridyl)methyl)amino methyl)-4-methylphenol (e). To 1.11 g (3.68 mmol) of (**d**) dissolved in 10 ml of dichloromethane, 1.00 ml (3.8 mmol) of $SOCl_2$ dissolved in 5 ml of dichloromethane was added dropwise over 30 min. After stirring at room temperature for 4 h, the solvent and remaining $SOCl_2$ was removed under vacuum. The remaining yellowish solid was dissolved in 6 ml of ethanol. This solution was added dropwise over 45 min to a solution of 0.787 g (2.28 mmol) of (**b**) in 18 ml ethanol and 2.5 ml of triethylamine. The reaction mixture was then refluxed for 1.5 h after which the solvent was removed under reduced pressure (rotary evaporator). The remaining solid was dissolved in aqueous phosphate buffer (0.1 M, pH 7) and extracted with 3 × 100 ml of dichloromethane. The organic phases were combined, dried over Na_2SO_4, filtered and evaporated to yield a brown crude product that was purified by chromatography on silica using a mixture of heptane, toluene and triethylamine (4 : 2 : 1) as eluent. This yielded 0.857 g (48.8%) of a yellowish product. ^{1}H NMR (500 MHz) $CDCl_3$: δ 8.50 (d, 1H, $J = 6.1$ Hz), 8.49 (d, 1H, $J = 5.9$ Hz) 7.61 (t, 2H, $J = 7.7$ Hz) 7.53 (d, 1H, $J = 7.3$ Hz) 7.42 (d, 1H, $J = 6.1$ Hz) 7.13 (t, 1H, $J = 4.3$ Hz) 7.11 (t, 1H, $J = 4.9$ Hz) 6.97 (s, 1H) 6.85 (s, 1H) 4.15 (q, 2H, $J = 7.1$H z) 3.95 (s, 2H) 3.83 (s, 2H) 3.76 (s, 2H) 3.73 (s, 2H) 3.38 (s, 2H) 3.03 (s, 1H) 2.21 (s, 3H) 1.24 (t, 3H, $J = 7.2$ Hz) 1.10 (d, 6H, $J = 4.4$ Hz).

2-(*N*-isopropyl-*N*-((2-pyridyl)methyl)aminomethyl)-6-(*N*-(carboxylmethyl)-*N*-((2-pyridyl)methyl)aminomethyl)-4-methylphenol H_4IPCPMP$(PF_6)_2\cdot 2H_2O$ (H_4L). To 0.925 g (1.941 mmol) of (**e**) dissolved in 12 ml of a 1 : 1 (v/v) ethanol–water mixture was added 5.83 ml of a 1.0 M NaOH(aq) solution (5.83 mmol) and the resultant solution was left stirring for 1.5 h. Then 1 M HCl (aq) was added dropwise until pH was 1–2 and thereafter 1.34 g (7.98 mmol) of $NaPF_6$ was added under stirring. The white precipitate formed was collected by filtration and washed three times with small amounts of cold water and then dried under vacuum in a dessicator overnight to yield 1.22 g (81.0%) of a white powder. Crystals of X-ray quality were grown from a mixture of methanol and water. ^{1}H-NMR (500 MHz) CD_3CN δ 8.48 (d, 1H, $J = 5.8$ Hz) 8.46 (d, 1H, $J = 4.8$ Hz) 8.25 (t, 1H, $J = 7.9$ Hz) 7.78 (t, 1H, $J = 7.8$ Hz) 7.73 (t, 1H, $J = 6.8$ Hz) 7.61 (d, 1H, $J = 8.0$ Hz) 7.34 (dd, 1H, $J = 5.3$ Hz, $J = 7.1$ Hz) 7.25 (d, 1H, $J = 7.8$ Hz) 6.93 (s, 2H) 4.35 (s, 2H, br) 4.18 (s, 2H, br) 4.09 (s, 2H) 3.83 (s, 2H) 3.69 (s, 2H) 3.68 (sept, 1H, $J = 6.6$ Hz) 2.14 (s, 3H) 1.44 (d, 6H, $J = 6.6$ Hz). IR (KBr) cm^{-1} 3680 (w, O–H), 3300 (s, br, O–H), 3118 (w, C–H *etc.*), 2987 (w, C–H *etc.*), 1710 (s, C=O), 1616 (m, C=C arom.), 1598 (m, C=C arom.), 1538 (m, C=C arom.), 1491 (m, C=C arom.), 1468 (m, C=C arom.), 1442 (m, C=C arom.), 1393 (m), 1229 (s, C–OH carbox. acid), 843 (*vs*, PF_6), 558 (s, PF_6). Elem. Anal. $C_{26}H_{36}F_{12}N_4O_4P_2$ Calc.: C, 41.17; H, 4.78; F, 30.06; N, 7.39; Found: C, 41.72; H, 5.264; F, 29.92; N, 8.008.

[{Zn_2(IPCPMP)(OAc)}$_2$][PF_6]$_2$ (2). A total of 30.1 mg (0.0388 mmol) of (H_4L) and 6.3 mg (0.12 mmol, 3 eq.) of sodium methoxide were dissolved in 0.9 ml methanol and then transferred to a solution of 18.7 mg (0.0852 mmol) zinc acetate dihydrate in 0.9 ml water. A white precipitate formed upon addition but it slowly dissolved again. A microcrystalline material (28 mg, 92%) was formed upon slow evaporation of solvent. Crystals suitable for X-ray crystallography were grown from methanol solution by slow evaporation.

[{Zn_2(IPCPMP)(OAc)}$_2$]$(PF_6)_2$ Elem. Anal. Calc. $C_{56}H_{66}F_{12}N_8O_{10}P_2Zn_4$ C, 43.04; H, 4.26; N, 7.17; Found C, 42.8; H 4.4; N, 7.0. IR (KBr) cm^{-1}: 2964 (w, C–H); 2921 (w, C–H); 1609 (s, *anti*-sym. –CO_2); 1598 (s, *anti*-sym. –CO_2); 1563 (m, C=C arom.); 1486 (m, C=C arom.); 1435 (m, sym. –CO_2); 1414 (m, sym. –CO_2); 844 (s); 559 (m); UV/vis (acetonitrile, nm): 234 (sh); 260; 298; FAB+ MS: *m*/*z* (^{64}Zn) 829 ([Zn_2(IPCPMP)$(OAc)_2$] + NB^+, NB^+ = 3-nitrobenzyl cation, matrix); 633 ([Zn_2(IPCPMP)(OAc)]$^+$); 619 ([Zn_2(IPCPMP)(O_2CH)]$^+$); 591 ([Zn_2(IPCPMP)(OH)]$^+$); 1411 ([{Zn_2(IPCPMP)(O_2CCH_3)}$_2$]$^{2+}\cdot PF_6^-$).

[Zn_2(IPCPMP)$(O_2CC(CH_3)_3)_2$][PF_6]$_2$ (3). A total of 30.0 mg (0.0386 mmol) of (H_4L) was dissolved in 1.0 ml ethanol. To this solution 12.1 mg (0.0888 mmol) $ZnCl_2$ and 9.7 mg (0.0782 mmol) sodium pivalate, each dissolved in 0.3 ml ethanol, were added. When 43.1 µl (0.3091 mmol) triethyl amine was added a white precipitate formed. This precipitate was filtered off and the remaining solution was left to slowly evaporate which yielded crystalline material.

[{Zn_2(IPCPMP)$(O_2CC(CH_3)_3$}$_2$]$(PF_6)_2\cdot 2H_2O$,$2C_2H_5OH$ Elem. Anal. Calc. $C_{64}H_{86}F_{12}N_8O_{12}P_2Zn_4$ C, 44.93; H, 5.07; N, 6.55; Found C, 44.5; H, 5.1; N, 6.4; IR (KBr) cm^{-1}: 2970 (w); 2921 (w); 2871 (w); 1609 (s, br, *anti*-sym. –CO_2); 1562 (m); 1482 (m); 1442 (w, sym. –CO_2); 1418 (m, sym. –CO_2); 844 (s); 553 (m); UV/vis (acetonitrile, nm): 233 (sh); 261; 298; FAB+ MS: *m*/*z* (^{64}Zn) 675 ([Zn_2(IPCPMP)$(O_2CC(CH_3)_3]^+$); 1495 ([{Zn_2(IPCPMP)$(O_2CC(CH_3)_3)$}$_2$]$^{2+}\cdot PF_6^-$).

X-Ray structure determinations†

The crystals of **2** and H_4L were immersed in cryo-oil, mounted in a Nylon loop, and measured at a temperature of 100 K. The X-ray diffraction data were collected on a Nonius KappaCCD diffractometer using Mo-Kα radiation ($\lambda = 0.71073$ Å). The *Denzo-Scalepack* or *EvalCCD* program packages were used for cell refinements and data reductions. The structures were solved by direct methods using the *SHELXS-97* programs[69] with the *WinGX* graphical user interface. A semi-empirical absorption correction (*SADABS* or Xprep in SHELXTL) was applied to all data. Structural refinements were carried out using *SHELXL-97*. In **2**, the H_2O, OH and NH hydrogen atoms were located from the difference Fourier map but constrained to ride on their

parent atom, with $U_{iso} = 1.5$. Other hydrogens were positioned geometrically and constrained to ride on their parent atoms, with C–H = 0.98–1.00 Å and $U_{iso} = 1.2–1.5\ U_{eq}$ (parent atom). The crystallographic details are summarized in Table 1. Bond lengths and angles for the organic framework of **2**, **3** and **H_4L** is displayed in Table 2 while selected hydrogen bonds for **H_4L** can be found in Table S1 (ESI).† Relevant distances and angles for the metal coordination in **2** and **3** are shown in Table 3. To allow easy comparison, the labels of the atoms for **2** and **3** have been renumbered to fit those of **H_4L** and hence are different from the labels in the CIF files already published.[22]

Potentiometric studies

The pH-potentiometric titrations were performed in the pH range 2.0–11.0 or until precipitation occurred on samples of 10.00 cm^3 at an ionic strength of 0.2 M (KCl) and at 25.0 ± 0.1 °C. During the titrations purified, strictly oxygen-free argon was continuously bubbled through the samples. Samples were always freshly prepared and since **H_4L** (H_4IPCPMP(PF_6)$_2$) was only slightly soluble in water, its maximum concentration, what could be used in the samples during the titrations, was 0.0015 M. The metal ion stock solutions were prepared from ZnO (Reanal) dissolved in a known amount of HCl solution (0.1 M). The concentration of the metal ion stock solution was determined gravimetrically *via* precipitation of quinolin-8-olates. The HCl concentration of the Zn(II) solution and the exact concentration of the carbonate-free KOH titrant were determined by pH-potentiometry. The metal to ligand ratios were, 1.5 : 1 and 2 : 1. The pH-metric titrations were performed with a Radiometer pHM84 instrument equipped with a Metrohm combined electrode (type 6.0234.100). Titrant KOH was added from a Metrohm 715 Dosimat auto burette. The electrode system was calibrated according to Irving *et al.*[70] so that the pH-meter readings could be directly converted into hydrogen ion concentration. The water ionization constant (pK_w) obtained was 13.75 ± 0.01. The pH-metric results were utilized to find the stoichiometry of species and to calculate the stability constants. The calculations were made with the aid of the computer program PSEQUAD.[71]

Electrospray mass spectrometric studies

Electrospray ionization time-of-flight mass spectrometric (ESI-TOF MS) analysis was carried out on a Bruker BIOTOF II ESI-TOF instrument and regular ESI measurements were carried out on a Brucker HCT Ultra instrument. The metal to ligand ratio was 2 : 1. For the Zn^{2+}-IPCPMP system, 0.0007 M ligand concentration at pH 7.80 was used. The solutions were introduced directly into the ESI source by a syringe pump (Cole-Parmer Ins. Comp. type 74900) at a flow rate of 2 μL h^{-1}. The temperature of drying gas (N_2) was 100 °C. The pressure of the nebulizating gas (N_2) was 30 psi. Voltages applied at the capillary entrance, capillary exit and the first and the second skimmers were –4500, 120, 40 and 30 V, respectively. The spectrum was accumulated and recorded by a digitalizer at a sampling rate of 2 GHz. The spectrometer was operated at unit mass resolution and was calibrated with sodium trifluoroacetate. For the measurements in absence of buffer, the pH values were adjusted with sodium hydroxide in a water–MeOH mixture (1 : 1 v/v). The solutions were introduced directly into the ESI source by a syringe pump (KD Scientific) at a flow rate of 200 μL min^{-1}. The temperature of the drying gas (N_2) was 300 °C. The pressure of the nebulizating gas (N_2) was 10 psi. The spectrometer was operated at Ultra Scan Mode and was calibrated with ESI Tuning Mix.

Kinetic measurements

The increase in concentration of the products, p-nitrophenol and 2,4-dinitrophenol, were monitored at 25 °C by UV/vis spectroscopy at 400 nm in quartz suprasil cuvettes using a Cary 300 Bio spectrophotometer equipped with a 12 position thermostated cell changer. Substrate and catalyst concentrations were 0.80 mM and 0.25 mM respectively and the ionic strength and pH were kept constant by using total concentrations of 0.1 M $NaClO_4$ and 0.01 M buffer (MES pH5-6.5, MOPS 7.0–7.5, EPPS 8.0–8.5, CHES 9.0–9.5, CAPS 10.0–11.0). The pH of the buffer was adjusted in standard solutions using a calibrated pH meter before addition to the cuvettes. Each cuvette was prepared by consecutive addition of 980 μl acetonitrile, 30 μl of a 0.0167 M standard solution of the complex in acetonitrile–H_2O (2 : 1 v/v) and 970 μl of a 0.0207 M buffer solution containing 0.207 M $NaClO_4$. After mixing, the zero absorption was measured. Then 20 μl of a 0.080 M standard solution of the substrate in H_2O was added and after quick mixing the increase in absorption over time was measured at 400 nm, initially every minute but after 4 h every 5 min and after 8 h every 15 min. The initial rates were calculated by fitting a straight line to the curve corresponding to abs < 5% of the maximum absorption at full conversion (usually the first 30 min). The dissociation constant of the phenol products ($pK_{a,PNP} = 7.15$, $pK_{a,BNP} = 4.07$) were taken into account when calculating the total concentration of phenol from the absorption of the phenolate at 400 nm ($\varepsilon_{PNP} = 18\,500\ M^{-1}\ cm^{-1}$, $\varepsilon_{BNP} = 12\,100\ M^{-1}\ cm^{-1}$). Complex and substrate concentration dependence were studied at pH 8.5 for both the BDNPP and HPNP cleavage. The measurement and preparation of the solutions in the cuvettes were made in the same manner as above with total $NaClO_4$ concentration 0.1 M but with total buffer concentration increased to 0.050 M. For the dependence on complex concentration different volumes of stock solution of [{Zn_2(IPCPMP)(OAc)}$_2$][PF_6]$_2$ (**2**) (2.0 mM) was added to yield total concentrations of 0.020, 0.050, 0.1, 0.25, 0.5 and 1.0 mM of the postulated dinuclear complex (**2***) in the cuvette while keeping the substrate concentration constant at 1.0 mM. The second order rate constant k_{2nd} was determined from the slope of the straight line fitted to the data, weighting each point by $1/\sigma^2$. The values are shown in Table 5. For the dependence on substrate concentration a similar addition of stock solutions of NaBDNPP (40.0 mM) and Ba(HPNP)$_2$ (20 mM) yielded total concentrations of 0.25, 0.5, 1.0, 2.0 4.0 and 6.0 mM in the cuvette while the complex concentration was kept constant at 0.050 mM. Initial rates were measured three times for each concentration as above and the results were fitted to the Michaelis–Menten equation weighting each point by $1/\sigma^2$ where σ is the standard deviation of each respective point. The fitted parameters K_M and V_{max} and their standard errors along with calculated values of K_{ass} and k_{cat} are shown in Table 5.

Acknowledgements

This research has been supported by a grant from the Swedish Research Council (VR), and has been carried out within the

framework of the International Research Training Group *Metal Sites in Biomolecules–Structures, Regulation and Mechanisms* (www.biometals.eu). We wish to thank Dr Luca Zuppiroli for assistance with the mass spectrometry measurements. E.Cs. and E.F. thank OTKA-NKTH CK77586 for financial support.

References

1 N. H. Williams, B. Takasaki, M. Wall and J. Chin, *Acc. Chem. Res.*, 1999, **32**, 485–493.
2 J. A. Cowan, *Chem. Rev.*, 1998, **98**, 1067–1088.
3 E. L. Hegg and J. N. Burstyn, *Coord. Chem. Rev.*, 1998, **173**, 133–165.
4 N. Sträter, W. N. Lipscomb, T. Klabunde and B. Krebs, *Angew. Chem., Int. Ed. Engl.*, 1996, **35**, 2024–2055.
5 D. E. Wilcox, *Chem. Rev.*, 1996, **96**, 2435–2458.
6 J. Weston, *Chem. Rev.*, 2005, **105**, 2151–2174.
7 R. H. Holm, P. Kennepohl and E. I. Solomon, *Chem. Rev.*, 1996, **96**, 2239–2314.
8 W. N. Lipscomb and N. Sträter, *Chem. Rev.*, 1996, **96**, 2375–2433.
9 M. M. Benning, H. Shim, F. M. Raushel and H. M. Holden, *Biochemistry*, 2001, **40**, 2712–2722.
10 P. J. O'Brien and D. Herschlag, *Biochemistry*, 2002, **41**, 3207–3225.
11 C. Romier, R. Dominguez, A. Lahm, O. Dahl and D. Suck, *Proteins: Struct., Funct., Genet.*, 1998, **32**, 414–424.
12 E. Hough, L. K. Hansen, B. Birknes, K. Jynge, S. Hansen, A. Hordvik, C. Little, E. Dodson and Z. Derewenda, *Nature*, 1989, **338**, 357–360.
13 G. Parkin, *Chem. Rev.*, 2004, **104**, 699–767.
14 B. N. Trawick, A. T. Daniher and J. K. Bashkin, *Chem. Rev.*, 1998, **98**, 939–960.
15 F. Mancin and P. Tecilla, *New J. Chem.*, 2007, **31**, 800–817.
16 M. Jarenmark, H. Carlsson and E. Nordlander, *C. R. Chim.*, 2007, **10**, 433–462.
17 R. Mitra, M. W. Peters and M. J. Scott, *Dalton Trans.*, 2007, 3924–3935.
18 M. Subat, K. Woinaroschy, C. Gerstl, B. Sarkar, W. Kaim and B. König, *Inorg. Chem.*, 2008, **47**, 4661–4668.
19 E. Kimura, *Curr. Opin. Chem. Biol.*, 2000, **4**, 207–213.
20 N. Mitic, S. J. Smith, A. Neves, L. W. Guddat, L. R. Gahan and G. Schenk, *Chem. Rev.*, 2006, **106**, 3338–3363.
21 H. Vahrenkamp, *Acc. Chem. Res.*, 1999, **32**, 589–596.
22 M. Jarenmark, S. Kappen, M. Haukka and E. Nordlander, *Dalton Trans.*, 2008, 993–996.
23 H. Carlsson, M. Haukka and E. Nordlander, *Inorg. Chem.*, 2002, **41**, 4981–4983.
24 H. Carlsson, M. Haukka and E. Nordlander, *Inorg. Chem.*, 2004, **43**, 5681–5687.
25 H. Carlsson, M. Haukka, A. Bousseksou, J. M. Latour and E. Nordlander, *Inorg. Chem.*, 2004, **43**, 8252–8262.
26 E. Lambert, B. Chabut, S. ChardonNoblat, A. Deronzier, G. Chottard, A. Bousseksou, J. P. Tuchagues, J. Laugier, M. Bardet and J. M. Latour, *J. Am. Chem. Soc.*, 1997, **119**, 9424–9437.
27 A. F. Abdel-Magid, K. G. Carson, B. D. Harris, C. A. Maryanoff and R. D. Shah, *J. Org. Chem.*, 1996, **61**, 3849–3862.
28 A. W. Addison, T. N. Rao, J. Reedijk, J. Vanrijn and G. C. Verschoor, *J. Chem. Soc., Dalton Trans.*, 1984, 1349–1356.
29 The structural index σ is defined as $\sigma = (\beta - \alpha)/60$, where α and β are the two largest angles around the metal (cf. ref. 28)..
30 C. J. Carrell, H. L. Carrell, J. Erlebacher and J. P. Glusker, *J. Am. Chem. Soc.*, 1988, **110**, 8651–8656.
31 A. S. Borovik, V. Papaefthymiou, L. F. Taylor, O. P. Anderson and L. Que, *J. Am. Chem. Soc.*, 1989, **111**, 6183–6195.
32 G. B. Deacon and R. J. Phillips, *Coord. Chem. Rev.*, 1980, **33**, 227–250.
33 S. Albedyhl, M. T. Averbuch-Pouchot, C. Belle, B. Krebs, J. L. Pierre, E. Saint-Aman and S. Torelli, *Eur. J. Inorg. Chem.*, 2001, 1457–1464.
34 P. Karsten, A. Neves, A. J. Bortoluzzi, M. Lanznaster and V. Drago, *Inorg. Chem.*, 2002, **41**, 4624–4626.
35 M. Lanznaster, A. Neves, A. J. Bortoluzzi, B. Szpoganicz and E. Schwingel, *Inorg. Chem.*, 2002, **41**, 5641–5643.
36 S. C. Batista, A. Neves, A. J. Bortoluzzi, I. Vencato, R. A. Peralta, B. Szpoganicz, V. V. E. Aires, H. Terenzi and P. C. Severino, *Inorg. Chem. Commun.*, 2003, **6**, 1161–1165.
37 R. Jovito, A. Neves, A. J. Bortoluzzi, M. Lanznaster, V. Drago and W. Haase, *Inorg. Chem. Commun.*, 2005, **8**, 323–327.
38 M. Lanznaster, A. Neves, A. J. Bortoluzzi, V. V. E. Aires, B. Szpoganicz, H. Terenzi, P. C. Severino, J. M. Fuller, S. C. Drew, L. R. Gahan, G. R. Hanson, M. J. Riley and G. Schenk, *JBIC, J. Biol. Inorg. Chem.*, 2005, **10**, 319–332.
39 A. Neves, M. Lanznaster, A. J. Bortoluzzi, R. A. Peralta, A. Casellato, E. E. Castellano, P. Herrald, M. J. Riley and G. Schenk, *J. Am. Chem. Soc.*, 2007, **129**, 7486–7487.
40 G. Schenk, R. A. Peralta, S. C. Batista, A. J. Bortoluzzi, B. Szpoganicz, A. K. Dick, P. Herrald, G. R. Hanson, R. K. Szilagyi, M. J. Riley, L. R. Gahan and A. Neves, *J. Biol. Inorg. Chem.*, 2008, **13**, 139–155.
41 Isolated tertiary amines commonly have pK_a values around 9–10; H. K. Hall, *J. Am. Chem. Soc.*, 1957, **79**, 5441–5444.
42 M. Jarenmark, H. Carlsson, V. Trukhan, M. Haukka, S. E. Canton, M. Walczak, W. Fullagar, V. Sundström and E. Nordlander, *Inorg. Chem. Commun.*, 2010, **13**, 334–337.
43 T. Gajda, R. Kramer and A. Jancso, *Eur. J. Inorg. Chem.*, 2000, 1635–1644.
44 O. Iranzo, A. Y. Kovalevsky, J. R. Morrow and J. P. Richard, *J. Am. Chem. Soc.*, 2003, **125**, 1988–1993.
45 C. Bazzicalupi, A. Bencini, A. Bianchi, V. Fusi, P. Paoletti, G. Piccardi and B. Valtancoli, *Inorg. Chem.*, 1995, **34**, 5622–5631.
46 C. He and S. J. Lippard, *J. Am. Chem. Soc.*, 2000, **122**, 184–185.
47 M. Gelinsky, R. Vogler and H. Vahrenkamp, *Inorg. Chem.*, 2002, **41**, 2560–2564.
48 U. Herr, W. Spahl, G. Trojandt, W. Steglich, F. Thaler and R. van Eldik, *Bioorg. Med. Chem.*, 1999, **7**, 699–707.
49 R. R. Buchholz, M. E. Etienne, A. Dorgelo, R. E. Mirams, S. J. Smith, S. Y. Chow, L. R. Hanton, G. B. Jameson, G. Schenk and L. R. Gahan, *Dalton Trans.*, 2008, 6045–6054.
50 B. Bauer-Siebenlist, F. Meyer, E. Farkas, D. Vidovic, J. A. Cuesta-Seijo, R. Herbst-Irmer and H. Pritzkow, *Inorg. Chem.*, 2004, **43**, 4189–4202.
51 B. Bauer-Siebenlist, F. Meyer, E. Farkas, D. Vidovic and S. Dechert, *Chem.–Eur. J.*, 2005, **11**, 4349–4360.
52 F. Meyer and P. Rutsch, *Chem. Commun.*, 1998, 1037–1038.
53 M. Y. Yang, O. Iranzo, J. P. Richard and J. R. Morrow, *J. Am. Chem. Soc.*, 2005, **127**, 1064–1065.
54 S. Acharya, A. Foldesi and J. Chattopadhyaya, *J. Org. Chem.*, 2003, **68**, 1906–1910.
55 I. M. Kolthoff and T. Kameda, *J. Am. Chem. Soc.*, 1931, **53**, 832–842.
56 S. Albedyhl, D. Schnieders, A. Jancso, T. Gajda and B. Krebs, *Eur. J. Inorg. Chem.*, 2002, 1400–1409.
57 K. Selmeczi, C. Michel, A. Milet, I. Gautier-Luneau, C. Philouze, J.-L. Pierre, D. Schnieders, A. Rompel and C. Belle, *Chem.–Eur. J.*, 2007, **13**, 9093–9106.
58 P. Molenveld, S. Kapsabelis, J. F. J. Engbersen and D. N. Reinhoudt, *J. Am. Chem. Soc.*, 1997, **119**, 2948–2949.
59 C. A. Bunton and S. J. Farber, *J. Org. Chem.*, 1969, **34**, 767–772.
60 G.-M. Yang, J. Li, Y.-W. Ren, H. Guo, M.-Y. Duan, F.-X. Zhang and X. Zhang, *Transition Met. Chem.*, 2009, **34**, 191–196.
61 C.-X. Yuan, Y.-B. Wei and P. Yang, *Chin. J. Chem.*, 2006, **24**, 1006–1012.
62 S.-I. Kondo, K. Shinbo, T. Yamaguchi, K. Yoshida and Y. Yano, *J. Chem. Soc., Perkin Trans. 2*, 2001, 128–131.
63 J. Kim and H. Lim, *Bull. Korean Chem. Soc.*, 1999, **20**, 491–493.
64 A. Greatti, M. Scarpellini, R. A. Peralta, A. Casellato, A. J. Bortoluzzi, F. R. Xavier, R. Jovito, M. Aires de Brito, B. Szpoganicz, Z. Tomkowicz, M. Rams, W. Haase and A. Neves, *Inorg. Chem.*, 2008, **47**, 1107–1119.
65 M. Jarenmark, Dinuclear metal complexes modelling active sites of metallohydrolases, PhD Thesis, Lund University, 2009.
66 C. Policar, F. Lambert, M. Cesario and I. Morgenstern-Badarau, *Eur. J. Inorg. Chem.*, 1999, 2201–2207.
67 D. M. Brown and D. A. Usher, *J. Chem. Soc.*, 1965, 6558–6565.
68 G. Rawji and R. M. Milburn, *J. Org. Chem.*, 1981, **46**, 1205–1206.
69 G. Sheldrick, *Acta Crystallogr., Sect. A: Found. Crystallogr.*, 2008, **64**, 112–122.
70 H. Irving, M. G. Miles and L. D. Pettit, *Anal. Chim. Acta*, 1967, **38**, 475–488.
71 L. Zékány and I. Nagypál in D. Legett (Ed.), *Computational Methods for the Determination of Stability Constants*, Plenum Press, New York, 1985.
72 C. F. Macrae, P. R. Edgington, P. McCabe, E. Pidcock, G. P. Shields, R. Taylor, M. Towler and J. van de Streek, *J. Appl. Crystallogr.*, 2006, **39**, 453–457.
73 L. Farrugia, *J. Appl. Crystallogr.*, 1997, **30**, 565.

